

## Production and identification of new neutron-rich nuclei, $^{31}\text{Ne}$ and $^{37}\text{Mg}$ , in the reaction $80\text{A MeV } ^{50}\text{Ti} + ^{181}\text{Ta}$

H. Sakurai,<sup>1</sup> N. Aoi,<sup>2</sup> A. Goto,<sup>1</sup> M. Hirai,<sup>2</sup> N. Inabe,<sup>1</sup> M. Ishihara,<sup>1,2</sup> H. Kobinata,<sup>2</sup> T. Kubo,<sup>1</sup> H. Kumagai,<sup>1</sup>  
T. Nakagawa,<sup>1</sup> T. Nakamura,<sup>2</sup> M. Notani,<sup>2</sup> Y. Watanabe,<sup>1</sup> Y. Watanabe,<sup>2</sup> and A. Yoshida<sup>1</sup>

<sup>1</sup>The Institute of Physical and Chemical Research (RIKEN), 2-1 Hirosawa, Wako, Saitama 351-01, Japan

<sup>2</sup>Department of Physics, University of Tokyo, 7-3-1 Hongo, Bunkyo, Tokyo 113, Japan

(Received 22 July 1996)

We report on the first production and identification of two neutron-rich nuclei  $^{31}\text{Ne}$  and  $^{37}\text{Mg}$ . They were produced in the projectile fragmentation of an 80A MeV  $^{50}\text{Ti}$  beam on a  $^{181}\text{Ta}$  target, and were efficiently analyzed and identified through the fragment separator RIPS at RIKEN, by measuring the magnetic rigidity, time of flight, energy loss, and total kinetic energy. The particle stability of the new isotopes is discussed in comparison with various mass predictions.

[S0556-2813(96)50312-2]

PACS number(s): 25.70.Mn, 21.10.Dr, 27.30.+t

Synthesis and identification of new isotopes towards the neutron drip line are essential for understanding the nuclear stability in an extreme condition of isospin asymmetry. While many recent works have greatly contributed to the synthesis of very neutron-rich nuclei, the drip line has been reached only for lighter isotopes below  $Z=10$ . This paper reports on another experimental attempt to extend the domain of nuclear synthesis particularly in the region of  $Z=10-12$ , and  $N\sim 20$ .

In this region, the most neutron-rich isotopes so far observed are  $^{32}\text{Ne}$  [1],  $^{35}\text{Na}$  [2], and  $^{36}\text{Mg}$  [3], where  $^{32}\text{Ne}$  and  $^{36}\text{Mg}$  were barely obtained by incorporating an enriched  $^{48}\text{Ca}$  beam for projectile fragmentation. Theoretically, various mass formulas [4,5] and phenomenological treatments [6] provide predictions on the location of the neutron drip line, but they disagree considerably with one another.

A particular aspect of neutron-rich isotopes around  $N=20$  is the tendency towards prolate deformation in spite of the effect of spherical stability due to magicity of the neutron number [7-11]. As a matter of fact, a large  $B(E2; 0^+ \rightarrow 2^+)$  value was recently observed for a  $N=20$  nucleus  $^{32}\text{Mg}$  [12], supporting the possibility of such deformation. It is argued [7-10] that the deformation may also account for the enhanced binding energies manifested by some of the known nuclei in this region [13-15]. With this respect we pay special attention to the stability of another  $N=20$  isotope,  $^{31}\text{Ne}$ . In a previous work [1], this nucleus was reported to be particle unstable in accordance with many mass formulas [4]. Meanwhile, some of the theoretical treatments [5,9,10] incorporating a deformation effect tend to predict particle stability of  $^{31}\text{Ne}$ .

In this work several ingredients were facilitated to enhance the yield rates of neutron-rich nuclei. First, a high-energy neutron-rich beam of 80A MeV  $^{50}\text{Ti}$  was employed to induce projectile-fragment reactions. While  $^{50}\text{Ti}$  is somewhat inferior to  $^{48}\text{Ca}$  in producing neutron-rich nuclei, use of a high-energy beam allowed us to adopt a thicker production target, resulting in improved statistics. Choice of  $^{181}\text{Ta}$  for the production target, which was made by following the results of systematic survey runs, was also helpful to increase

the yields. Among others, use of the RIKEN projectile-fragment separator (RIPS) [16] was most powerful in collecting these products with its large acceptances for momentum (6%) and solid angle (5 msr) as well as the sizable maximum magnetic rigidity of 5.76 Tm. With all of these effects combined, yield rates of about 1 order of magnitude higher than in similar experiments [1,3] were achieved.

$^{50}\text{Ti}$  ions provided by the ECR ion source with 60% enriched  $^{50}\text{Ti}$ -oxide powder were accelerated at the RIKEN Ring Cyclotron. The production yields of very neutron-rich nuclei strongly depend on the  $N/Z$  ratios of the target nuclei, possibly due to an effect of transfer reactions [1,17]. We thus performed a supplementary experiment in order to compare the production yields between two energy-loss-equivalent targets,  $^9\text{Be}$  and  $^{181}\text{Ta}$ , with thicknesses of 289 and 435 mg/cm<sup>2</sup>, respectively. The thicknesses were chosen according to a theoretical estimation in which the INTENSITY code of Ref. [18] was used to predict secondary beam intensities and the production rates were optimized for  $A/Z\sim 3.1$  nuclei. We found that for nuclei of  $Z\sim 10$  and  $A/Z\sim 3$ ,  $^{181}\text{Ta}$  produces about twice the yields of  $^9\text{Be}$  at this beam energy. On this basis, we employed the  $^{181}\text{Ta}$  target to search for new neutron-rich isotopes.

The reaction fragments were collected and analyzed with the RIPS spectrometer operated in the achromatic mode [16]. Figure 1 shows a schematic layout of the RIPS. Taking into account the energy loss in the target for both the beam and fragments with  $A/Z\sim 3.1$ , the magnetic rigidity of the RIPS spectrometer was set to be 3.6 Tm. Particle identification was performed event by event, by measuring the magnetic rigidity ( $B\rho$ ), time of flight (TOF), energy loss ( $\Delta E$ ), and total kinetic energy (TKE) [19].

Positions of fragments at the momentum dispersive focal plane (F1) were measured using a parallel plate avalanche chamber (PPAC) in order to determine the  $B\rho$  value (see Fig. 1). The sensitive area of the PPAC was 10 cm(W) $\times$ 10 cm(H), which covered a wide rigidity acceptance of 4.2%. To minimize  $\delta$ -ray effects causing worse position resolutions,  $\text{C}_3\text{F}_8$  gas, which yields rather large stopping powers for  $\delta$  rays, was utilized for the PPAC. Furthermore, position

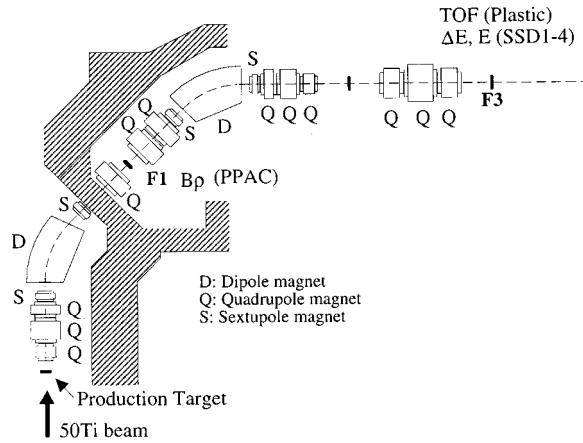


FIG. 1. Experimental setup for the production and identification of new neutron-rich isotopes at the RIKEN-RIPS spectrometer.

measurements by two independent  $x$ -projective cathodes of the PPAC helped to reject spurious position information caused by the  $\delta$  rays. The gas was circulated at a pressure of 9 Torr, and the total thickness was about  $2 \text{ mg/cm}^2$ , where the energy loss of the fragments was negligibly small (less than 0.1% of the total kinetic energies). Each  $x$ -projective cathode had 1 mm pitch strips, and the particle positions were determined via a charge division method. The efficiency was over 90% for  $Z \sim 10$  nuclei. The position resolution was about 3.5 mm in rms, which corresponds to 0.15% accuracy of the  $B\rho$  measurements.

All of the other detectors were located at the final focal point (F3), involving a 0.5 mm thick plastic scintillation counter (PL), two 0.3 mm surface barrier type silicon detectors (SSD1, SSD2), and two 3 mm thick lithium drift silicon detectors (SSD3, SSD4). The TOF of each fragment over the 27.5 m flight path between the target and F3 was determined from the PL timing and RF signal of the cyclotron. The first three silicon detectors provided three independent  $\Delta E$  measurements and all the silicon detectors combined provided a TKE measurement.

The measured values of  $B\rho$ , TOF,  $\Delta E$ , and TKE were combined to give redundant particle identifications, as described in Refs. [19,20]. The proton number ( $Z$ ) of a fragment was determined from the total  $\Delta E$  at the first three silicon detectors and from the TOF. The  $Z$  distributions have asymmetric shapes with tails on the high  $Z$  side, which is mainly due to a pile-up effect of light fragments. The accuracy in the  $Z$  determination ( $\sigma_Z$ ) was obtained to be about 0.8% (rms) for  $Z \sim 10$  nuclei by fitting the  $Z$  distributions to a Gaussian form. The mass-to-charge ratio ( $A/Q$ ) of a fragment was determined with an accuracy of 0.2% in rms from the  $B\rho$  and TOF, while the charge ( $Q$ ) was obtained with an accuracy of 2% from the TKE,  $B\rho$ , and TOF. It is probable that those fragments that were not fully ionized were subject to being misidentified as more neutron-rich nuclei. Hence, we selectively employed fully stripped fragments by imposing a condition of  $|Z - Q|/Z < 5\%$ . This condition was satisfied only by those fragments that stopped at the SSD4 and therefore provided correct  $Q$  values from the TKE information.

Figure 2(a) shows a two-dimensional plot,  $A/Z$  versus

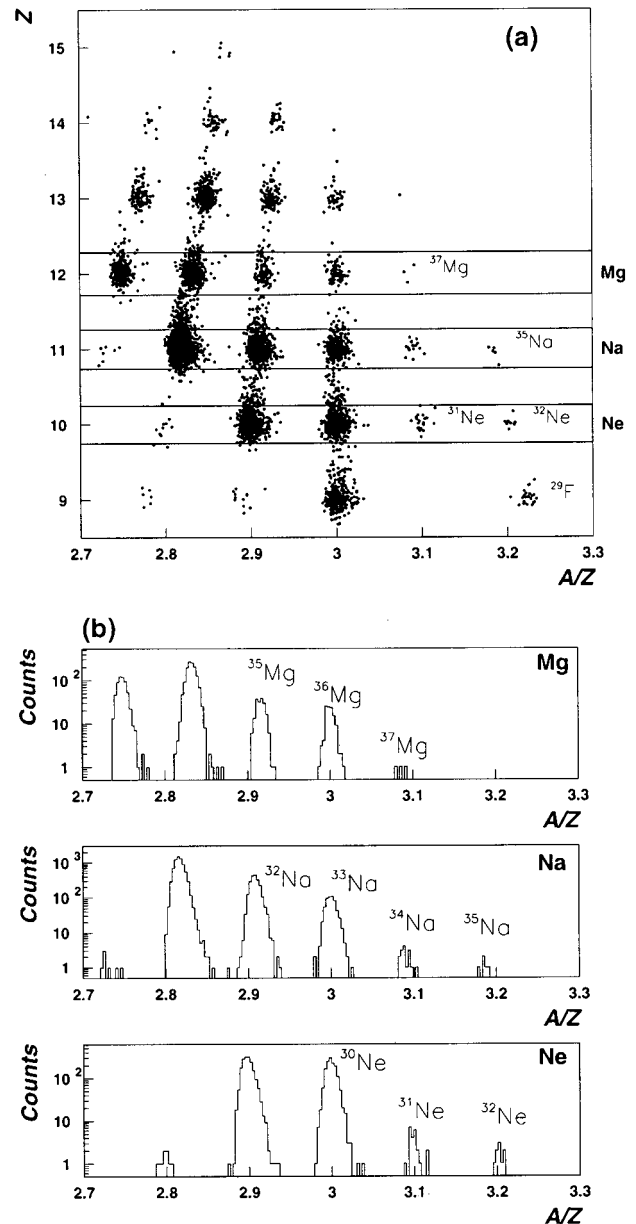


FIG. 2. (a) Two-dimensional  $A/Z$  versus  $Z$  plot and (b) yield spectrum as a function of  $A/Z$  for Ne, Na, and Mg isotopes, which were obtained in the reaction of the  $^{50}\text{Ti}$  beam at 80A MeV on a  $435 \text{ mg/cm}^2$  tantalum target during a four-day run with a magnetic rigidity of 3.6 Tm of the RIPS spectrometer. The  $^{31}\text{Ne}$  isotope (23 counts) and  $^{37}\text{Mg}$  (3 counts) are clearly visible. In the two-dimensional plot (a), the  $Z$ -window for each isotope is shown for the yield distributions (b). From the charge distributions, we determined the accuracies for  $Z$  ( $\sigma_Z$  rms) to be 0.85%, 0.8%, and 0.76% for Ne, Na, and Mg, respectively. The  $Z$ -window width corresponds to  $6\sigma_Z$ .

$Z$ , while Fig. 2(b) illustrates the yield spectrum as a function of  $A/Z$  for Ne, Na and Mg isotopes. The  $Z$ -windows of  $6\sigma_Z$  width indicated in Fig. 2(a) were applied to obtain the yield spectrum (b). The window width chosen covered about 95% of events for  $A/Z \sim 3$  fragments. The results were obtained from the data accumulated for four days with an average beam intensity of  $\sim 2 \text{ pA}$ . All of the fragments of  $^{30,31,32}\text{Ne}$ ,  $^{32,33,34,35}\text{Na}$ , and  $^{35,36,37}\text{Mg}$  were stopped at the

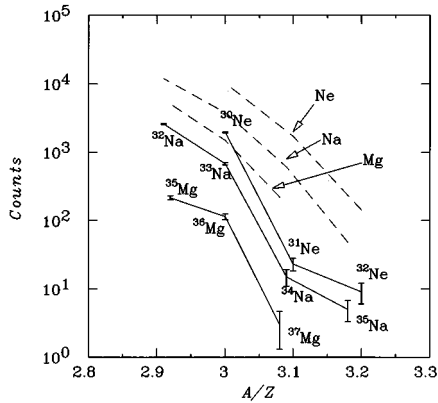


FIG. 3. Systematic trends of the production yields as a function of  $A/Z$ , for the very neutron-rich isotopes of Ne, Na, and Mg. The experimental conditions are the same as described in Fig. 2. The dashed curves indicate the predicted yields for each isotope by the INTENSITY code [18]. No significant drops of yields are observed for either  $^{31}\text{Ne}$  or  $^{37}\text{Mg}$ , compared to the trend concerning Na isotope yields.

SSD4 with the selected window of the magnetic rigidity. Significant numbers of events have been observed for new isotopes,  $^{31}\text{Ne}$  (23 events) and  $^{37}\text{Mg}$  (three events). We have also observed nine events of  $^{32}\text{Ne}$ . In addition one event that could possibly be associated with  $^{40}\text{Al}$  was obtained. A previous work [1] reported four events of  $^{32}\text{Ne}$ , in harmony with the present result. On the other hand, Ref. [1] showed that no events associated with  $^{31}\text{Ne}$  could be found at a  $B\rho$  setting for  $A/Z \sim 3.25$  nuclei, leading to an inference that  $^{31}\text{Ne}$  is unbound. The discrepancies with our result could be caused by differences in the statistics, transmission due to the different  $B\rho$  settings, or resolving power in fragment identification. In the present experiment the  $B\rho$  measurement was additionally incorporated. Good quality of the resolving power is indicated in Fig. 2(a) by, e.g., absence of  $^{28}\text{F}$ , which is known to be unbound.

Figure 3 shows systematic behaviors of the production yields as a function of  $A/Z$ . The experimental data are the same as for Fig. 2 while the theoretical curves (dotted lines) are due to the INTENSITY code of Ref. [18]. Two aspects are noted for the experimental data: (1) the curves for different isotopes tend to be parallel to each other, and (2) even-odd staggering is apparent. The lack of significant drops in the observed yields at  $^{31}\text{Ne}$  and  $^{37}\text{Mg}$  suggests that the half-lives of these nuclei are not much smaller than the flight time of about 260 ns, and hence that they are particle stable.

The theoretical curves overestimate the yields of these very neutron-rich nuclei by 1–2 orders of magnitude. In the calculation, an empirical formula for production cross sections of fragments [21] was used. The formula was originally obtained based on the data for isotopes rather close to the stability line. Modification for the case of very neutron-rich nuclei needs to be investigated.

The particle stability found for  $^{31}\text{Ne}$  and  $^{37}\text{Mg}$  implies that their one- and two-neutron separation energies are positive. Since these nuclei are  $Z$ -even and  $N$ -odd nuclei, their one-neutron separation energies ( $S_{1n}$ ) are more important in terms of particle stability. To observe the systematic behaviors of  $S_{1n}$  for these very neutron-rich nuclei, we show in

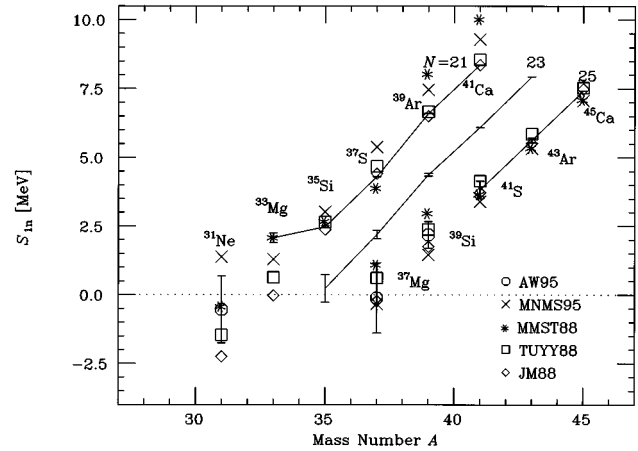


FIG. 4. Systematics for the one-neutron separation energies ( $S_{1n}$ ) for even- $Z$  and  $N=21, 23$ , and  $25$  nuclei as a function of the mass number ( $A$ ) [22]. Our experiment gives the  $S_{1n}$  values of larger than 0 MeV for  $^{31}\text{Ne}$  and  $^{37}\text{Mg}$ . The measured  $S_{1n}$  data are taken from Ref. [23], and are connected by the solid lines. The open circles show the  $S_{1n}$  values from the systematic mass extrapolation by Audi and Wapstra (AW95) [23]. The errors of the extrapolation are also shown. Presented are the  $S_{1n}$  values for  $N=21$  and  $25$  nuclei from the following mass predictions: three macroscopic-and-microscopic models by Möller *et al.* (MMST88) [24], by Tachibana *et al.* (TUY88) [25], and by Möller *et al.* (MNMS95) [5], and the Garvey-Kelson formula by Jänecke and Masson (JM88) [26].

Fig. 4 a so-called Yamada-Matsumoto plot [22] of the measured  $S_{1n}$  values [23] for  $N=21, 23$ , and  $25$  nuclei as a function of the mass number ( $A$ ). Only even- $Z$  nuclei are employed to eliminate any even-odd effects on the nuclear masses. For comparison, Fig. 4 also presents the values of  $S_{1n}$  for  $N=21$  and  $25$  nuclei based on the systematic mass extrapolation using the measured masses by Audi and Wapstra (AW95) [23], together with the theoretical predictions of four mass formulas: three macroscopic-microscopic models based on the finite-range droplet model by Möller *et al.* (MMST88) [24], on the liquid drop model by Tachibana *et al.* (TUY88) [25], and on the finite-range liquid-drop model recently developed by Möller *et al.* (MNMS95) [5], and the Garvey-Kelson model by Jänecke-Masson (JM88) [26]. AW95 predicts that the  $S_{1n}$  values for  $^{31}\text{Ne}$  and  $^{37}\text{Mg}$  are  $-0.53 \pm 1.22$  MeV and  $-0.12 \pm 1.28$  MeV, respectively. These predictions are consistent with our result. The particle stability of  $^{37}\text{Mg}$  is well predicted by all four mass formulas: the  $S_{1n}$  of  $^{37}\text{Mg}$  is positive, or very close to the particle threshold. No exotic aspects are shown in terms of particle stability.

On the other hand, concerning the stability of  $^{31}\text{Ne}$ , the experimental results are consistent only with two models: MMST88 and MNMS95. If the curve of the measured  $S_{1n}$  for  $N=21$  decreases smoothly as  $A$  decreases like the  $N=23$  curve,  $^{31}\text{Ne}$  would be unbound, as predicted by the other two models. However, the curve does not decrease smoothly, but has a sudden increase at  $^{33}\text{Mg}$ . This behavior is predicted by MMST88 and MNMS95. These models include the nuclear deformation effect for both the macroscopic and microscopic parts, and they show that  $^{31}\text{Ne}$  is bound or barely unbound.

Deformation effects on the enhanced binding energies for  $Z \approx 11$  and  $N \approx 20$  nuclei have been also argued by different microscopic theories [7–10]. Among them, two theories predict the particle stability of  $^{31}\text{Ne}$ : a relativistic mean field theory (RMF) [9] and a shell model by Poves and Retamosa (PR) [10]. It should be noted that both theories require a large deformation effect to explain the known ground-state spins of  $^{29,31}\text{Na}$ . The RMF theory has shown that the neutron-rich Ne, Na, and Mg nuclei are highly deformed, which helps to explain the enhanced binding energies. This theory predicts that the  $S_{1n}$  value of  $^{31}\text{Ne}$  is 0.40 MeV. The PR shell model suggests that a large configuration mixing in the neutron valence space extended to the fp shell orbits results in large deformation, which leads to the enhanced binding energies, and the  $S_{1n}$  value of 0.75 MeV for  $^{31}\text{Ne}$ .

Both the mass formulas and the microscopic theories demonstrate that the stability of  $^{31}\text{Ne}$  can be related to an enhanced binding energy due to a deformation effect.

In summary, we have produced and identified the new neutron-rich nuclei  $^{31}\text{Ne}$  and  $^{37}\text{Mg}$  from the reaction 80A MeV  $^{50}\text{Ti} + ^{181}\text{Ta}$  at the RIKEN-RIPS, by means of measuring the magnetic rigidity, time of flight, energy loss, and total kinetic energy. This experiment has shown for the first time that  $^{31}\text{Ne}$  and  $^{37}\text{Mg}$  are particle-bound nuclei.

Our sincere gratitude is extended to the staffs of the RIKEN Ring Cyclotron for their operation of the accelerator. One of the authors (M.N.) acknowledges support from the Junior Technology Research Associate of the Institute of Physical and Chemical Research.

- 
- [1] D. Guillemaud-Mueller *et al.*, Phys. Rev. C **41**, 937 (1990).  
 [2] M. Langevin *et al.*, Phys. Lett. **125B**, 116 (1983).  
 [3] D. Guillemaud-Mueller *et al.*, Z. Phys. A **332**, 189 (1989).  
 [4] *1986-1987 Atomic Mass Predictions*, edited by P.E. Hausteijn [At. Data Nucl. Data Tables **39**, 185 (1988)].  
 [5] P. Möller, J.R. Nix, W.D. Myers, and W.J. Swiatecki, At. Data Nucl. Data Tables **59**, 185 (1995).  
 [6] I. Tanihata, D. Hirata, and H. Toki, Nucl. Phys. **A583**, 769c (1995).  
 [7] X. Campi, H. Flocard, A.K. Kerman, and S. Koonin, Nucl. Phys. **A251**, 193 (1975).  
 [8] E.K. Warburton, J.A. Becker, and B.A. Brown, Phys. Rev. C **41**, 1147 (1990).  
 [9] S.K. Patra and C.R. Praharaaj, Phys. Lett. B **273**, 13 (1991).  
 [10] A. Poves and J. Retamosa, Nucl. Phys. **A571**, 221 (1994).  
 [11] N. Fukunishi, T. Otsuka, and T. Sebe, Phys. Lett. B **296**, 279 (1992).  
 [12] T. Motobayashi *et al.*, Phys. Lett. B **346**, 9 (1995).  
 [13] C. Thibault *et al.*, Nucl. Phys. **A251**, 193 (1975).  
 [14] N.A. Orr *et al.*, Phys. Lett. B **258**, 29 (1991).  
 [15] X.G. Zhou *et al.*, Phys. Lett. B **260**, 285 (1991).  
 [16] T. Kubo *et al.*, Nucl. Instrum. Methods Phys. Res. B **70**, 309 (1992).  
 [17] D. Guerreau, Nucl. Phys. **A447**, 37c (1985).  
 [18] J.A. Winger, B.M. Sherrill, and D.J. Morrissey, Nucl. Instrum. Methods Phys. Res. B **70**, 380 (1992).  
 [19] M.F. Mohar *et al.*, Phys. Rev. Lett. **66**, 1571 (1991).  
 [20] D. Bazin *et al.*, Nucl. Phys. **A515**, 349 (1990).  
 [21] K. Sümmerer *et al.*, Phys. Rev. C **42**, 2546 (1990).  
 [22] M. Yamada and Z. Matsumoto, J. Phys. Soc. Jpn. **16**, 1497 (1961).  
 [23] G. Audi and A.H. Wapstra, Nucl. Phys. **A595**, 409 (1995).  
 [24] P. Möller, W.D. Myers, W.J. Swiatecki, and J. Treiner, At. Data Nucl. Data Tables **39**, 225 (1988).  
 [25] T. Tachibana, M. Uno, M. Yamada, and S. Yamada, At. Data Nucl. Data Tables **39**, 251 (1988).  
 [26] J. Jänecke and P.J. Masson, At. Data Nucl. Data Tables **39**, 265 (1988).